

An explicit reconstruction algorithm for the transverse ray transform of a second rank tensor field from three axis data.

Naeem M. Desai

William R.B. Lionheart

November 18, 2015

Abstract

We give an explicit plane-by-plane filtered back-projection reconstruction algorithm for the transverse ray transform of symmetric second rank tensor fields on Euclidean 3-space, using data from rotation about three orthogonal axes. We show that in the general case two axis data is insufficient but give an explicit reconstruction procedure for the potential case with two axis data.

1 Introduction

The transverse ray transform (TRT) of rank two symmetric tensor fields in three dimensional Euclidean space has recently been shown to be of importance in x-ray diffraction strain tomography [5], however currently reconstruction algorithms are known only for data from rotations about six axes [8, Sec 5.1.6] or complete data [5]. Given that, in the proposed application, each projection is acquired laboriously using a raster scan, it is advantageous to perform the reconstruction using data from a minimum number of axes and making the most of the data collected from each projection. In this paper we give an explicit reconstruction formula for three axis data using similar techniques to those employed by [4] for the *truncated* transverse ray transform (TTRT). The inversion formula uses plane-by-plane filter and back-projection operations familiar from inversion of the parallel x-ray transform of a scalar field. We go on to show that data from only two rotation axes are insufficient in the general case, but give an explicit reconstruction for the potential case with two axis data. We present some numerical results for our reconstruction algorithms using simulated data.

2 Definitions and notation

We denote the complex vector space of symmetric \mathbb{R} -bilinear maps $\mathbb{R}^3 \times \mathbb{R}^3 \rightarrow \mathbb{C}$ by $S^2\mathbb{C}^3$. The elements of this space are (*complex-valued*) symmetric tensors of second rank on \mathbb{R}^3 . We will identify a complex symmetric tensor $f \in S^2\mathbb{C}^3$ with the \mathbb{C} -linear operator, $f : \mathbb{C}^n \rightarrow \mathbb{C}^n$, as usual $\langle f\xi, \eta \rangle = \langle f\eta, \xi \rangle = f(\xi, \eta)$ where $\eta, \xi \in \mathbb{R}^3$.

Defining the Schwartz space of rapidly decreasing functions $\mathcal{S}(\mathbb{R}^n)$ on n -dimensional Euclidean ($n = 2$ or 3) space in the usual way, we extend this definition to (complex) vector fields $\mathcal{S}(\mathbb{R}^n; \mathbb{C}^n)$ and complex symmetric tensor fields as $\mathcal{S}(\mathbb{R}^n; S^2\mathbb{C}^n)$. The choice of Schwartz spaces and the use of complex vectors and tensors is convenient as we will rely heavily on the Fourier transform. Extension to Sobolev spaces for compactly supported fields follows using the usual apparatus as applied to scalar ray transforms [7]. We define the Fourier transform $F : \mathcal{S}(\mathbb{R}^3) \rightarrow \mathcal{S}(\mathbb{R}^3)$, by

$$F[f] = \hat{f}(y) = (2\pi)^{-3/2} \int_{\mathbb{R}^3} e^{-i\langle y, x \rangle} f(x) dx.$$

Given an orthonormal basis (e_1, e_2, e_3) of \mathbb{R}^3 , a tensor $f \in S^2\mathbb{C}^3$ can be represented by the symmetric 3×3 matrix $(f_{jk}), f_{jk} = f(e_j, e_k)$. The Hermitian scalar product on $S^2\mathbb{C}^3$ can be written as $\langle f, g \rangle = \sum_{j,k=1}^3 f_{jk} \bar{g}_{jk}$ independently of the choice of an orthonormal basis. Since only orthonormal bases will be used in this paper, we do not distinguish between co- and contravariant tensors.

We will need the partial Fourier transform $F_V : \mathcal{S}(\mathbb{R}^3) \rightarrow \mathcal{S}(\mathbb{R}^3)$, for any k -dimensional vector subspace $V \subset \mathbb{R}^3$. Given Cartesian coordinates (x_1, x_2, x_3) in \mathbb{R}^3 such that

$V = \{x | x_{k+1} = \dots = x_3 = 0\}$, the partial Fourier Transform can be written as

$$F_V[f] = \hat{f}(y_1, \dots, y_k, x_{k+1}, \dots, x_3) = (2\pi)^{-k/2} \int_{\mathbb{R}^k} e^{-i(y_1 x_1 + \dots + y_k x_k)} f(x) dx_1 \dots dx_k.$$

This result is independent of the choice of orthonormal coordinates and satisfies the commutation law $F = F_V F_{V^\perp} = F_{V^\perp} F_V$.

The *oriented* lines in \mathbb{R}^3 can be parameterized by points of the tangent bundle of the unit sphere \mathbb{S}^2 in \mathbb{R}^3

$$TS^2 = \{(\xi, x) \in \mathbb{R}^3 \times \mathbb{R}^3 \mid |\xi| = 1, \langle \xi, x \rangle = 0\} \subset \mathbb{R}^3 \times \mathbb{R}^3.$$

An oriented line $l \subset \mathbb{R}^3$ is uniquely represented as $l = \{x + t\xi \mid t \in \mathbb{R}\}$ with $(\xi, x) \in TS^2$. The Schwartz space $\mathcal{S}(TS^2)$ is defined as in [4].

Our main object of interest is the Transverse Ray Transform (TRT) of symmetric rank two tensor fields

$$J : \mathcal{S}(\mathbb{R}^3; S^2\mathbb{C}^3) \rightarrow \mathcal{S}(TS^2; S^2\mathbb{C}^3),$$

which is defined by

$$Jf(\xi, x) = \int_{-\infty}^{\infty} P_\xi f(x + t\xi) dt, \quad (1)$$

where $P_\xi : S^2\mathbb{C}^3 \rightarrow S^2\mathbb{C}^3$ is the orthogonal projection onto the subspace $\{f \in S^2\mathbb{C}^3 \mid f\xi = 0\}$.

For example, for an orthonormal basis of the form $(e_1, e_2, e_3 = \xi)$, the projection is expressed by

$$P_\xi f = \begin{pmatrix} f_{11} & f_{12} & 0 \\ f_{12} & f_{22} & 0 \\ 0 & 0 & 0 \end{pmatrix}. \quad (2)$$

By contrast the scalar x-ray transform (or simply the ray transform) of a function $f \in \mathcal{S}(\mathbb{R}^3)$ is defined by

$$Xf(\xi, x) = \int_{-\infty}^{\infty} f(x + t\xi) dt.$$

We also have the Longitudinal Ray Transform (LRT),

$$I : \mathcal{S}(\mathbb{R}^3; \mathbb{C}^3) \rightarrow \mathcal{S}(T\mathbb{S}^2), \quad I : \mathcal{S}(\mathbb{R}^3; S^2\mathbb{C}^3) \rightarrow \mathcal{S}(T\mathbb{S}^2),$$

defined on vector and tensor fields respectively by

$$If(\xi, x) = \int_{-\infty}^{\infty} \langle f(x + t\xi), \xi \rangle dt, \quad If(\xi, x) = \int_{-\infty}^{\infty} \langle f(x + t\xi)\xi, \xi \rangle dt. \quad (3)$$

The x-ray transform and LRT can also be defined on a plane in \mathbb{R}^3 . For $\eta \in \mathbb{S}^2$, let $\eta^\perp = \{\xi \in \mathbb{R}^3 \mid \langle \xi, \eta \rangle = 0\}$, $\mathbb{R}\eta = \{s\eta \mid s \in \mathbb{R}\}$, $\eta_{\mathbb{C}}^\perp$ be the complexification of η^\perp and $\mathbb{S}_\eta^1 = \{\xi \in \eta^\perp \mid |\xi| = 1\}$ be the unit sphere in η^\perp . Given $s \in \mathbb{R}$, let $s\eta + \eta^\perp$ be the plane through $s\eta$ parallel to η^\perp and $\iota_{s,\eta} : s\eta + \eta^\perp \subset \mathbb{R}^3$ be the identical embedding. The family of oriented lines in the plane $s\eta + \eta^\perp$ is parameterized by points of the manifold $T\mathbb{S}_\eta^1 = \{(\xi, x) \mid \xi \in \mathbb{S}_\eta^1, x \in \eta^\perp, \langle \xi, x \rangle = 0\}$ such that a point $(\xi, x) \in T\mathbb{S}_\eta^1$ corresponds to the line $\{s\eta + x + t\xi \mid t \in \mathbb{R}\}$. We define the X-ray transform on a plane $X_{\eta,s}f(\xi, x)$ and the LRT on the plane $s\eta + \eta^\perp$

$$X_{\eta,s} : \mathcal{S}(s\eta + \eta^\perp; \mathbb{C}) \rightarrow \mathcal{S}(T\mathbb{S}_\eta^1) \quad (4)$$

$$I_{\eta,s} : \mathcal{S}(s\eta + \eta^\perp; \eta_{\mathbb{C}}^\perp) \rightarrow \mathcal{S}(T\mathbb{S}_\eta^1) \quad (5)$$

$$I_{\eta,s} : \mathcal{S}(s\eta + \eta^\perp; S^2\eta_{\mathbb{C}}^\perp) \rightarrow \mathcal{S}(T\mathbb{S}_\eta^1) \quad (6)$$

by the following formulae

$$X_{\eta,s}f(\xi, x) = \int_{-\infty}^{\infty} f(s\eta + x + t\xi) dt, \quad (7)$$

$$I_{\eta,s}f(\xi, x) = \int_{-\infty}^{\infty} \langle f(s\eta + x + t\xi), \xi \rangle dt, \quad (8)$$

$$I_{\eta,s}f(\xi, x) = \int_{-\infty}^{\infty} \langle f(s\eta + x + t\xi)\xi, \xi \rangle dt \quad (9)$$

respectively. One can see that operators (3) and (9) are related. If $f \in \mathcal{S}(\mathbb{R}^3; S^2\mathbb{C}^3)$ and $\iota_{\eta,s}^*f$ is the slice of f by the plane $s\eta + \eta^\perp$, then $I_{\eta,s}(\iota_{\eta,s}^*f)(\xi, x) = If(\xi, s\eta + x)$, for $(\xi, x) \in T\mathbb{S}_\eta^1$.

A typical experimental situation would involve rotation of the specimen (or equivalently the source and detector) about some finite collection of axes. In the scalar case of the x-ray transform rotation about one axis is sufficient as the problem reduces to the Radon transform in the plane, for a family of planes normal to the rotation axis. Consider first the case $n = 2$ in which X is identical to the Radon transform. In this case the formal adjoint $B = X^* : \mathcal{S}(T\mathbb{S}^1) \rightarrow C^\infty(\mathbb{R}^2)$, the back-projection operator, is well defined and given by

$$B\phi(x) = \frac{1}{2\pi} \int_{\mathbb{S}^1} \phi(\xi, \langle \xi, x \rangle) d\xi \quad (10)$$

for $\phi \in \mathcal{S}(T\mathbb{S}^1)$. We then have the inversion formula [7] for data $\phi(\xi, x) = X_{\eta, s}f(\xi, x)$ in the range of X

$$F[f(x)](y) = |y|F[B\phi(x)], \quad (11)$$

which means that inversion is performed by a *ramp filter* (also known as a Riesz potential) applied to the back-projected data.

This operation can be performed *slice by slice* to invert the x-ray transform for $n = 3$, in which case data is needed only for $\xi \in \eta^\perp$ for some fixed *rotation axis* $\eta \in \mathbb{S}^2$. In this case the slice-by-slice back-projection operator $B_\eta : \mathcal{S}(\mathbb{R} \times T\mathbb{S}_\eta^1) \rightarrow C^\infty(\mathbb{R}^3)$. The reconstruction formula (11) becomes

$$F_{\eta^\perp}[f(x)](s, y) = |\Pi_\eta y|F_{\eta^\perp}[B_\eta\phi(x)], \quad (12)$$

where $s = \langle x, \eta \rangle$.

Notice that the component $\langle \eta, Jf(\xi, x)\eta \rangle = X\langle \eta, f\eta \rangle(x, \xi)$, for $\xi \in \eta^\perp$ is simply the scalar x-ray transform in the plane through x normal to η . As observed in [8, Sec 5.1.6] this component can be reconstructed using any inversion formula for the planar Radon transform inversion plane by plane, including the one given in (12). Choosing six rotation axes η_i so that the outer products $\eta\eta^T$ are linearly independent in $S^2\mathbb{R}^3$ recovers f everywhere. As mentioned in the introduction this procedure is likely to be time-consuming as rotations are performed about six axes and yet for each ray only one measurement (out of a possible three) is used. The aim of this paper is to show, via a constructive inversion procedure, that f can be determined uniquely from the data $Jf(x, \xi)$ for $\xi \in e_i^\perp$, $i = 1, \dots, 3$. Of course the diagonal elements f_{ii} are already determined as above so our main task is to provide a reconstruction procedure for the off-diagonal elements.

For a given rotation axis η and direction $\xi \in \eta^\perp$ we have in addition to the ‘axial’ component $\langle \eta, Jf(\xi, x)\eta \rangle$ the ‘non axial’ components $\langle \zeta, Jf(\xi, x)\eta \rangle$ where $\zeta = \xi \times \eta$ and $\langle \zeta, Jf(\xi, x)\zeta \rangle$ with which to reconstruct the off-diagonal (in a basis including η) elements of f .

3 Relations between transforms

The aim of this section is to write the non-axial components of $Jf(\xi, x)$, $\xi \in \eta^\perp$ in terms of longitudinal ray transforms on transaxial planes.

We have $P_\xi(f) = \Pi_\xi f \Pi_\xi$ where Π_ξ is the orthogonal projection matrix onto ξ^\perp , and the ‘off diagonal’ component can be expressed as

$$\begin{aligned} \langle (Jf)(\xi, x)\eta, \xi \times \eta \rangle &= \int_{-\infty}^{\infty} \langle \Pi_\xi f(x + t\xi) \Pi_\xi \eta, \xi \times \eta \rangle dt \\ &= \int_{-\infty}^{\infty} \langle f(x + t\xi)\eta, \xi \times \eta \rangle dt = \int_{-\infty}^{\infty} \langle \eta \times f(x + t\xi)\eta, \xi \rangle dt. \end{aligned}$$

Since the vector field $\eta \times f\eta$ is orthogonal to η , its restriction to every plane $s\eta + \eta^\perp$ can be considered as a vector field on the plane, i.e., $(\eta \times f\eta)|_{s\eta + \eta^\perp} \in \mathcal{S}(s\eta + \eta^\perp; \eta_\mathbb{C}^\perp)$.

As this is then contracted with the ray direction ξ we have

$$I_{\eta,s}((\eta \times f\eta)|_{s\eta+\eta^\perp})(\xi, x) = \langle (Jf)(\xi, x)\eta, \xi \times \eta \rangle \quad \text{for } (\xi, x) \in TS_\eta^1. \quad (13)$$

As we have seen in (2), that the TRT depends only on the projection normal to the direction of the ray. Now working in $(\eta, \zeta = \xi \times \eta, \xi)$ coordinates, let us consider, $\langle Jf(\xi, x)\zeta, \zeta \rangle$, which can be transformed into

$$\langle Jf(\xi, x)\zeta, \zeta \rangle = \int_{-\infty}^{\infty} \langle f(x + t\xi)\zeta, \zeta \rangle \, dt. \quad (14)$$

Let us parameterize ξ in the usual sense as

$$\xi = \begin{pmatrix} \cos \theta \\ \sin \theta \\ 0 \end{pmatrix}, \quad \text{so,} \quad \zeta = \begin{pmatrix} -\sin \theta \\ \cos \theta \\ 0 \end{pmatrix}.$$

Since $\zeta \in \xi^\perp$ we can calculate

$$\begin{aligned} \langle \zeta, f\zeta \rangle &= (-\sin \theta, \cos \theta, 0) \begin{pmatrix} f_{11} & f_{12} & 0 \\ f_{12} & f_{22} & 0 \\ 0 & 0 & 0 \end{pmatrix} \begin{pmatrix} -\sin \theta \\ \cos \theta \\ 0 \end{pmatrix} \\ &= f_{22} \cos^2 \theta - 2f_{12} \cos \theta \sin \theta + f_{11} \sin^2 \theta \\ &= (\cos \theta, \sin \theta, 0) \begin{pmatrix} f_{22} & -f_{12} & 0 \\ -f_{12} & f_{11} & 0 \\ 0 & 0 & 0 \end{pmatrix} \begin{pmatrix} \cos \theta \\ \sin \theta \\ 0 \end{pmatrix} \\ &= \xi \text{Adj}_{e_3^\perp}(f)\xi, \end{aligned}$$

where $\text{Adj}_{e_3^\perp}(f)$ denotes the adjugate matrix of the slice of f restricted to the plane; of course this is nothing other than the conjugation of $P_{e_3}f$ with a right angle rotation about the e_3 axis. Hence using the above, we see that for $\xi \in \eta^\perp$

$$\begin{aligned} \langle Jf(\xi, x)\zeta, \zeta \rangle &= \int_{-\infty}^{\infty} \langle f(x + t\xi)\zeta, \zeta \rangle \, dt \\ &= \int_{-\infty}^{\infty} \langle \text{Adj}_{\eta^\perp}(f)(x + t\xi)\xi, \xi \rangle = \langle I\text{Adj}_{\eta^\perp}(f)(\xi, x)\xi, \xi \rangle, \end{aligned} \quad (15)$$

which is the LRT transform of the two dimensional adjugate of the slice of f restricted to the plane. We notice that this is also exactly the transverse ray transform in the planar case. The results of this section can be summarized in the following Lemma:

Lemma 1 *Let $f \in \mathcal{S}(\mathbb{R}^3; S^2\mathbb{C}^3)$ be a symmetric tensor field. The equations*

$$I_{\eta,s}((\eta \times f\eta)|_{s\eta+\eta^\perp}) = (J_{\eta,s}^1 f), \quad (16)$$

$$I_{\eta,s}(\text{Adj}_{\eta^\perp}(\iota_{\eta,s}^* f)) = (J_{\eta,s}^2 f), \quad (17)$$

hold for every $s \in \mathbb{R}$ and $\eta \in \mathbb{S}^2$, where

$$(J_{\eta,s}^1 f) = \langle (Jf)(\xi, s\eta + x)\eta, \xi \times \eta \rangle, \quad (J_{\eta,s}^2 f) = \langle (Jf)(\xi, s\eta + x)\zeta, \zeta \rangle.$$

In the next section, we will transform (16) and (17) to algebraic equations by applying the Fourier transform to back-projected data.

4 Main algebraic equations

4.1 Curl Components of Tensor and Vector Fields

We can now transform (16) and (17) to algebraic equations by applying the Fourier transform. We only require what [8] refers to as tangential component $\tau g \in C^\infty(\mathbb{R}^2)$ of a vector field $g \in C^\infty(\mathbb{R}^2; \mathbb{C}^2)$, which is defined by

$$(\tau g)(y) = \langle g(y), y^\perp \rangle. \quad (18)$$

Here the vector y^\perp is the result of rotating y by $\pi/2$ in the positive direction. Of course, one can understand (18) as the $2D$ curl of a vector field in Fourier (frequency) space. The manifold $T\mathbb{S}^1$ can be identified with $\mathbb{R} \times \mathbb{S}^1$ by the diffeomorphism $(p, \xi) \mapsto (\xi, p\xi^\perp)$ for $(p, \xi) \in \mathbb{R} \times \mathbb{S}^1$. Therefore the derivative $\frac{\partial}{\partial p} : \mathcal{S}(T\mathbb{S}^1) \rightarrow \mathcal{S}(T\mathbb{S}^1)$ is well defined. For a vector field $f \in \mathcal{S}(\mathbb{R}^2; \mathbb{C}^2)$, the tangential component of the Fourier Transform $F[f]$ is recovered by the LRT, If , by the formula

$$\tau F[f] = \frac{i}{2}|y|F\left[B\left(\frac{\partial(If)}{\partial p}\right)\right]. \quad (19)$$

We see in [4] and [9], the tangential component, $\tau g \in C^\infty(\mathbb{R}^2)$, of a tensor field $g \in C^\infty(\mathbb{R}^2; S^2\mathbb{C}^2)$ is defined by

$$(\tau g)(y) = |y|^2 \text{tr } g - \langle g(y)y, y \rangle. \quad (20)$$

This is exactly the Fourier transform of the single unique non-zero component of the compatibility tensor of Barré de Saint-Venant in the plane

$$W(f) = \frac{\partial^2 f_{11}}{\partial x_2^2} - 2\frac{\partial^2 f_{12}}{\partial x_1 \partial x_2} + \frac{\partial^2 f_{22}}{\partial x_1^2}, \quad (21)$$

which is also sometimes described as the curl of a symmetric tensor field. For $f \in \mathcal{S}(\mathbb{R}^2; S^2\mathbb{C}^2)$, the tangential component of the Fourier transform $F[f]$ is recovered from the LRT, If , as

$$\tau F[f] = \frac{1}{2}|y|^3 F[B(If)]. \quad (22)$$

For $\phi \in \mathcal{S}(T\mathbb{S}^1)$, the function $B\phi(x)$ is C^∞ -smooth and bounded on \mathbb{R}^2 but does not decay fast enough to be in the Schwartz class. Thus we understand the Fourier transform in the distribution sense in (19) and (22).

4.2 Derivation of System of Equations

Let $f \in \mathcal{S}(\mathbb{R}^3; S^2\mathbb{C}^3)$ be a symmetric tensor field and denote by $f' = F_{\eta^\perp}[f] \in \mathcal{S}(\mathbb{R}^3; S^2\mathbb{C}^3)$ the partial Fourier transform of f . For any $s \in \mathbb{R}$, the restriction of the vector field $\eta \times f'\eta$ to the plane $s\eta + \eta^\perp$ coincides with the 2D Fourier transform of $(\eta \times f\eta)|_{s\eta + \eta^\perp}$. This is $(\eta \times f'\eta)|_{s\eta + \eta^\perp} = F_{\eta^\perp}[(\eta \times f\eta)|_{s\eta + \eta^\perp}]$.

We then apply formula (19) to the vector field $(\eta \times f\eta)|_{s\eta + \eta^\perp}$, giving

$$\tau((\eta \times f\eta)|_{s\eta + \eta^\perp})(s\eta + y) = \frac{i}{2}|y|F_{\eta^\perp} \left[B_\eta \left(\frac{\partial(I_{\eta,s}((\eta \times f\eta)|_{s\eta + \eta^\perp}))}{\partial p} \right) \right] \quad \text{for } y \in \eta^\perp, \quad (23)$$

Using (16), we can transform (23) giving

$$\tau((\eta \times f'\eta)|_{s\eta + \eta^\perp})(s\eta + y) = \frac{i}{2}|y|F_{\eta^\perp} \left[\left(B_\eta \frac{\partial(J_\eta^1 f)}{\partial p} \right) (s\eta + x) \right], \quad (24)$$

Note that (18) gives

$$\tau((\eta \times f'\eta)|_{s\eta + \eta^\perp})(s\eta + y) = \langle \eta \times f'(s\eta + y)\eta, \eta \times y \rangle = \langle f'(s\eta + y)\eta, y \rangle. \quad (25)$$

Upon substitution of (25) into the LHS of (24) and applying the one-dimensional Fourier transform $F_{\mathbb{R}\eta}$ taking s to σ gives

$$\langle \hat{f}(\sigma\eta + y')\eta, y' \rangle = \frac{i}{2}|y'|F \left[\left(B_\eta \frac{\partial(J_\eta^1 f)}{\partial p} \right) (s\eta + x') \right] \quad \text{for } y' \in \eta^\perp, \quad (26)$$

where \hat{f} is the three-dimensional Fourier transform $F[f]$. Since $y' \in \eta^\perp$ and $\sigma \in \mathbb{R}$, we let $y = \sigma\eta + y'$, where $y' = \Pi_\eta y$. Hence the previous formula (26) can be written as

$$\langle \hat{f}(y)\eta, \Pi_\eta y \rangle = \frac{i}{2}|\Pi_\eta y|F \left[\left(B_\eta \frac{\partial(J_\eta^1 f)}{\partial p} \right) (x) \right], \quad (27)$$

Note that (27) is identical to the off-diagonals for the TTRT operator case in [4]. Moreover this will just reconstruct the solenoidal part of the off-diagonals since the Fourier transform interweaves with the solenoidal part. For any $s \in \mathbb{R}$, the slice $\iota_{\eta,s}^* f'$ coincides with the 2D Fourier transform of the slice $\iota_{\eta,s}^* f$, i.e., $\iota_{\eta,s}^* f' = F_{\eta^\perp}[\iota_{\eta,s}^* f]$, where the Fourier transform on the plane $s\eta + \eta^\perp$. Henceforth, we refer to the adjugate of the slice of f' restricted to the plane as $\text{Adj}_{\eta^\perp}(\iota_{\eta,s}^* f') = h'$. Upon application of formula (22) to h' , we see

$$[\tau(h')](s\eta + y) = \frac{1}{2}|y|^3 F_{\eta^\perp} [B_\eta(I_{\eta,s}(\text{Adj}_{\eta^\perp}(\iota_{\eta,s}^* f')))] \quad \text{for } y \in \eta^\perp. \quad (28)$$

Using Lemma 1 we can rewrite the above as

$$[\tau(h')](s\eta + y) = \frac{1}{2}|y|^3 F_{\eta^\perp} [B_\eta(J_\eta^2 f)(s\eta + x)] \quad \text{for } y \in \eta^\perp, \quad (29)$$

Now, we apply formula (20) to the field $g = h' \in \mathcal{S}(s\eta + \eta^\perp; S^2\eta_\mathbb{C}^\perp)$ to give

$$[\tau(h')](s\eta + y) = |y|^2 \text{tr } h'(s\eta + y) - \langle h'(s\eta + y)y, y \rangle \quad \text{for } y \in \eta^\perp. \quad (30)$$

Next, substitute (30) into (29) to give

$$|y|^2 \text{tr } h'(s\eta + y) - \langle h'(s\eta + y)y, y \rangle = \frac{1}{2} |y|^3 F_{\eta^\perp}[B_\eta(J_\eta^2 f)(s\eta + x)] \quad \text{for } y \in \eta^\perp. \quad (31)$$

By applying the one-dimensional Fourier transform on $\mathbb{R}\eta$ to the above, we obtain

$$|y'|^2 \text{tr } \hat{h}(\sigma\eta + y') - \langle \hat{h}(\sigma\eta + y')y', y' \rangle = \frac{1}{2} |y'|^3 F[B_\eta(J_\eta^2 f)(s\eta + x')], \quad (32)$$

for $y \in \eta^\perp$. As before, employing a change of variables, $y = \sigma\eta + y'$, transforms the above to

$$|\Pi_\eta y|^2 \text{tr } \hat{h}(y) - \langle \hat{h}(y)\Pi_\eta y, \Pi_\eta y \rangle = \frac{1}{2} |\Pi_\eta y|^3 F[B_\eta(J_\eta^2 f)(x)], \quad \text{for } y \in \mathbb{R}^3. \quad (33)$$

In the following statement, the results are summarized.

Lemma 2 *Let \hat{f} be the 3D Fourier transform of a symmetric tensor field $f \in \mathcal{S}(\mathbb{R}^3; S^2\mathbb{C}^3)$. For a unit vector $\eta \in \mathbb{S}^2$, the following equations hold with the additional condition that $\hat{h} \in \mathcal{S}(\mathbb{R}^2; S^2\mathbb{C}^2)$, is defined to be the 2D adjugate of f restricted to the plane*

$$\langle \hat{f}(y)\eta, \Pi_\eta y \rangle = \lambda_\eta(y) \quad \text{and} \quad (34)$$

$$|\pi_\eta y|^2 \text{tr } \hat{h}(y) - \langle \hat{h}(y)\Pi_\eta y, \Pi_\eta y \rangle = \mu_\eta(y), \quad (35)$$

hold on \mathbb{R}^3 , with the right hand sides defined by

$$\lambda_\eta(y) = \frac{i}{2} |\Pi_\eta y| F \left[\left(B_\eta \frac{\partial(J_\eta^1 f)}{\partial p} \right) (x) \right], \quad (36)$$

$$\mu_\eta(y) = \frac{1}{2} |\Pi_\eta y|^3 F[B_\eta(J_\eta^2 f)(x)]. \quad (37)$$

The partial derivative $\frac{\partial}{\partial p} : \mathcal{S}(\mathbb{R} \times T\mathbb{S}_\eta^1) \rightarrow \mathcal{S}(\mathbb{R} \times T\mathbb{S}_\eta^1)$ is defined with the help of the diffeomorphism $\mathbb{R}^2 \times \mathbb{S}_\eta^1 \rightarrow \mathbb{R} \times \mathbb{R} \times T\mathbb{S}_\eta^1$, $(s, p, \xi) \mapsto (s, \xi, p\xi \times \eta)$. Given the data $Jf|_{\eta^\perp}$, right-hand sides $\lambda_\eta(y)$ and $\mu_\eta(y)$ of equations (34) - (35) can be effectively recovered by formulas (36) - (37).

Consider the case where $\eta = \eta_1 = (1, 0, 0)$. So $\Pi_\eta y = (0, y_2, y_3)$, $\hat{f}\eta = (\hat{f}_{11}, \hat{f}_{12}, \hat{f}_{13})$. To abbreviate formulas further, let us denote λ_{η_i} by λ_i and μ_{η_i} as μ_i . We use the orthonormal basis vectors e_1, e_2 and e_3 for η (i.e. $\eta_1 = e_1, \eta_2 = e_2$ and $\eta_3 = e_3$). With the aid of (34) and (36), we obtain a system of equations

$$\begin{pmatrix} y_2 & y_3 & 0 \\ y_1 & 0 & y_3 \\ 0 & y_1 & y_2 \end{pmatrix} \begin{pmatrix} \hat{f}_{12} \\ \hat{f}_{13} \\ \hat{f}_{23} \end{pmatrix} = \begin{pmatrix} \lambda_1 \\ \lambda_2 \\ \lambda_3 \end{pmatrix}. \quad (38)$$

The system of equations (38) can be solved to give

$$\hat{f}_{12} = \frac{\lambda_1}{2y_2} + \frac{\lambda_2}{2y_1} - \frac{\lambda_3 y_3}{2y_1 y_2}, \quad (39)$$

$$\hat{f}_{13} = \frac{\lambda_1}{2y_3} + \frac{\lambda_3}{2y_1} - \frac{\lambda_2 y_2}{2y_1 y_3}, \quad (40)$$

$$\hat{f}_{23} = \frac{\lambda_2}{2y_3} + \frac{\lambda_3}{2y_2} - \frac{\lambda_1 y_1}{2y_2 y_3}. \quad (41)$$

The result is summarized in the following theorem

Theorem 1 *A symmetric tensor field $f \in \mathcal{S}(\mathbb{R}^3; S^2 \mathbb{C}^3)$ is uniquely determined by the data $Jf(\xi, x)$ for $\xi \in \eta_i^\perp$, $i = 1, 2, 3$ where (η_1, η_2, η_3) forms an orthogonal basis.*

5 Alternative formulae for diagonal components

While the diagonal components f_{ii} are easily determined as we have seen, there is an alternative more complicated procedure to recover them. As this uses different data it can also be viewed as a compatibility condition on the three axis data.

Consider (35) and (37). When $\eta = e_1$, we have $\text{tr} \hat{h} = \hat{f}_{22} + \hat{f}_{33}$, and

$$\hat{h} = \begin{pmatrix} 0 & 0 & 0 \\ 0 & \hat{f}_{33} & -\hat{f}_{23} \\ 0 & -\hat{f}_{23} & \hat{f}_{22} \end{pmatrix}.$$

In the same manner as above (λ_i), we achieve a system of equations for μ_i

$$\begin{aligned} (y_2^2 + y_3^2)(\hat{f}_{22} + \hat{f}_{33}) - (y_2^2 \hat{f}_{33} - 2y_2 y_3 \hat{f}_{23} + y_3^2 \hat{f}_{22}) &= \mu_1, \\ (y_1^2 + y_3^2)(\hat{f}_{11} + \hat{f}_{33}) - (y_1^2 \hat{f}_{33} - 2y_1 y_3 \hat{f}_{13} + y_3^2 \hat{f}_{11}) &= \mu_2, \\ (y_1^2 + y_2^2)(\hat{f}_{11} + \hat{f}_{22}) - (y_1^2 \hat{f}_{22} - 2y_1 y_2 \hat{f}_{12} + y_2^2 \hat{f}_{11}) &= \mu_3. \end{aligned} \quad (42)$$

Rearranging the above gives the following

$$\begin{pmatrix} 0 & y_2^2 & y_3^2 \\ y_1^2 & 0 & y_3^2 \\ y_1^2 & y_2^2 & 0 \end{pmatrix} \begin{pmatrix} \hat{f}_{11} \\ \hat{f}_{22} \\ \hat{f}_{33} \end{pmatrix} = \begin{pmatrix} \mu_1 - 2y_2 y_3 \hat{f}_{23} \\ \mu_2 - 2y_1 y_3 \hat{f}_{13} \\ \mu_3 - 2y_1 y_2 \hat{f}_{12} \end{pmatrix}. \quad (43)$$

Let us relabel the RHS of the above as

$$\begin{pmatrix} \mu_1 - 2y_2 y_3 \hat{f}_{23} \\ \mu_2 - 2y_1 y_3 \hat{f}_{13} \\ \mu_3 - 2y_1 y_2 \hat{f}_{12} \end{pmatrix} = \begin{pmatrix} \nu_1 \\ \nu_2 \\ \nu_3 \end{pmatrix}. \quad (44)$$

In this way the solution of (43) can be written as

$$\hat{f}_{11} = \frac{1}{2y_1^2}(\nu_2 + \nu_3 - \nu_1),$$

$$\begin{aligned}\hat{f}_{22} &= \frac{1}{2y_2^2}(\nu_1 + \nu_3 - \nu_2), \\ \hat{f}_{33} &= \frac{1}{2y_3^2}(\nu_2 + \nu_1 - \nu_3).\end{aligned}\tag{45}$$

Upon substitution of the off-diagonals and μ 's into (45), we obtain

$$\begin{aligned}\hat{f}_{11} &= \frac{1}{2y_1^2}(\mu_2 + \mu_3 - \mu_1 + y_2\lambda_2 + y_3\lambda_3 - 3y_1\lambda_1), \\ \hat{f}_{22} &= \frac{1}{2y_2^2}(\mu_1 + \mu_3 - \mu_2 + y_1\lambda_1 + y_3\lambda_3 - 3y_2\lambda_2), \\ \hat{f}_{33} &= \frac{1}{2y_3^2}(\mu_2 + \mu_1 - \mu_3 + y_2\lambda_2 + y_1\lambda_1 - 3y_3\lambda_3).\end{aligned}\tag{46}$$

6 Insufficiency for two axes

To reduce the data acquisition time, experimentalists would want to rotate the specimen on its axis as few times as possible. We show that in the general case two orthogonal axes are insufficient by considering components in the null space of the TRT. Thus $J_\eta f = 0$. If we had two orthogonal axes, say $\eta = e_1, e_2$, then $\langle \eta, J_\eta f \rangle = 0$. This implies that $f_{11} = f_{22} = 0$. From the definition of $\lambda_\eta(y)$ and $\mu_\eta(y)$, $\lambda_1 = \lambda_2 = 0$ and $\mu_1 = \mu_2 = 0$. The system of equations for the off-diagonals (38) gives us

$$y_2\hat{f}_{12} + y_3\hat{f}_{13} = \lambda_1 = 0,\tag{47}$$

$$y_1\hat{f}_{12} + y_3\hat{f}_{23} = \lambda_2 = 0.\tag{48}$$

Moreover the system of equations corresponding to the other *non-axial* components, (44), gives

$$y_2^2\hat{f}_{22} + y_3^2\hat{f}_{33} = \mu_1 - 2y_2y_3\hat{f}_{23},\tag{49}$$

$$y_1^2\hat{f}_{11} + y_3^2\hat{f}_{33} = \mu_2 - 2y_1y_3\hat{f}_{13}.\tag{50}$$

Due to the argument at the start we can rearrange (50) as

$$y_3^2\hat{f}_{33} = -2y_2y_3\hat{f}_{23},\tag{51}$$

$$y_3^2\hat{f}_{33} = -2y_1y_3\hat{f}_{13}.\tag{52}$$

From the above, say \hat{f}_{33} is arbitrary and consequently \hat{f}_{13} and \hat{f}_{23} are determined as

$$\hat{f}_{23} = -\frac{y_3}{2y_2}\hat{f}_{33} \text{ and } \hat{f}_{13} = -\frac{y_3}{2y_1}\hat{f}_{33}.\tag{53}$$

Using the values obtained in (53) and substituting into (48) we can write \hat{f}_{12} as

$$\hat{f}_{12} = \frac{y_3^2}{2y_1y_2}\hat{f}_{33}.\tag{54}$$

Thus all the off-diagonal components in the tensor field are determined through \hat{f}_{33} which is arbitrary. Hence two axes are insufficient.

7 Potential cases

In the potential case $f_{ij} = \partial u_i / \partial x_j + \partial u_j / \partial x_i$ where $u \in \mathcal{S}(\mathbb{R}^3; \mathbb{C}^3)$. This is important for applications in that a linear strain tensor f has this form where u is twice the displacement field.

Without loss of generality suppose that data is known only for rotations about $\eta = e_1, e_2$. We have immediately f_{11}, f_{22} and hence by direct integration twice u_1 and u_2 . We now also have f_{12} from the partial derivatives of u_1 and u_2 . It remains only to find u_3 . Multiplying \hat{f}_{12} by $y_1 y_2$ and \hat{f}_{13} by $y_1 y_3$ and adding both of them in (41) gives

$$y_1 y_2 \hat{f}_{12} + y_1 y_3 \hat{f}_{13} = y_1 \lambda_1. \quad (55)$$

This gives us f_{13} in terms of known data and as $\partial u_1 / \partial x_3$ is known we have $\partial u_3 / \partial x_1$ and hence u_3 . We summarise in the theorem

Theorem 2 *A potential $f \in \mathcal{S}(\mathbb{R}^3; S^2(\mathbb{C}^3))$ is determined uniquely from $Jf(\xi, x)$ restricted to $\xi \in \eta_1^\perp$ and $\xi \in \eta_2^\perp$ where η_1 and η_2 are orthogonal.*

This result is of considerable practical importance as it means that strain tensors, in a scheme such as that envisaged in [5], can be recovered from rotations about only two axes.

We now show that in general a potential f cannot be recovered uniquely from a one-axis rotation by constructing a general element of the null space. Suppose we rotate only about e_1 we have immediately $f_{11} = 0$ and as $\hat{f}_{ij} = y_i \hat{u}_j + y_j \hat{u}_i$ we see $u_1 = 0$. Now as λ_1 and u_1 are zero

$$y_2 \hat{u}_2 + y_3 \hat{u}_3 = \frac{(\lambda_1 - (y_2^2 + y_3^2) \hat{u}_1)}{y_1} = 0. \quad (56)$$

and as $\mu_1 = 0$

$$y_2 \hat{u}_2 + y_3 \hat{u}_3 = \frac{\mu_1}{2(y_2^2 + y_3^2)} = 0, \quad (57)$$

giving no new information. So u must satisfy $u_1 = 0$ and $\partial u_2 / \partial x_2 + \partial u_3 / \partial x_3 = 0$. For example if u_2 is arbitrarily specified, then

$$u_3 = - \int_{-\infty}^{\infty} \frac{\partial u_2}{\partial x_2} dx_3. \quad (58)$$

8 Numerical results

8.1 Forward model

In order to generate data sets, we need to implement a discretized version of the operator J described in (1) as a matrix which will calculate integrals of projections and act upon generated strain fields represented by an array. Instead of calculating the whole matrix, we generate it one row at a time (on the *fly*) which corresponds to one individual source-detector pair for one of the three components in $P_\xi f$ described by (2).

8.1.1 Discrete representation of the tensor field

The discretized tensor field is stored as a $N \times N \times N \times 6$ vector, containing the 6 distinct values of the symmetric second rank tensor field for each voxel in a $N \times N \times N$ voxel grid. We increment first by the tensor component number, then the position x_1 , x_2 and finally x_3 . Furthermore, the data is represented by a $3 \times n_\theta \times h \times w \times 3$ multi-dimensional array (5 dimensional), where we use 3 rotation axes ($\eta = e_1, e_2$ and e_3), n_θ angles steps for tomographic acquisition around each axis and $h \times w$ represents how many rays in the horizontal and vertical direction. The factor of 3 is the number of independent values of Jf in (2) which we integrate along each ray.

8.1.2 Methodology

We simulate an experimental setup with parallel rays passing through a specimen. Sources and detectors consist of arrays in an equally spaced grid, either side of the object being scanned. The ratio of the number of rays in the horizontal to vertical direction is 4 : 3. The source-detector pair is kept fixed and the object is rotated. We follow the procedure of [10, Chapter 5.1.4] to calculate the approximate integral along a line through a voxel grid. This will give us the contribution of each voxel to the total integral for a given ray. For a given tensor we need to calculate the projection on to the plane perpendicular to the ray. To simplify this, we rotate the coordinate system. We extract the two appropriate components (relating to the axial and non-axial components). Since we have the contribution of each voxel to the integral, the length of intersection of the ray with the voxel, from ray tracing we can form the sum of these intersection lengths with the voxel values to form the approximate integral.

For our numerical experiments, phantoms were generated inside a cubic grid measuring $405 \times 405 \times 405$ voxels and measurements were simulated for a source/detector grid with 405×540 pixels. The number of rays in the vertical direction was taken to be the image height (i.e. 405 pixels). The pixel grid was then down-sampled by a factor of 3 to 135×180 pixels by the process of binning. Finally 1% Gaussian pseudo-random noise was added before reconstructing on a courser voxel grid measuring $135 \times 135 \times 135$. The number of angles (projections) was 240 per rotation axis.

8.2 Generating Phantoms

For input into the forward projector we generate two different phantoms or test fields. The first one only has smooth features and is expected to be less sensitive to algorithmic instabilities. The second phantom contains sharp edges and is designed to highlight the limitations of the explicit reconstruction algorithm for discontinuous strain fields.

8.2.1 Phantom 1: smooth

Phantom 1 is constructed from smooth Gaussians which makes it relatively easy to reconstruct. We define a cubic domain $[-1, 1]^3$ on which the components of f are supported, defined by 3-dimensional Gaussians $b_\alpha(x)$ for each of the components f_{ij}

according to Table 1, where

$$b_\alpha(x) = \alpha \exp(-50|x - a|^2).$$

Table 1: Phantom 1 - Smooth

f_{ij}	α	a_1	a_2	a_3
f_{11}	-1	-0.5	-0.5	-0.5
	1	-0.5	0.5	-0.5
	-1	-0.5	0.5	0.5
f_{12}	1	0.5	-0.5	0.5
	-1	0.5	0.5	-0.5
f_{13}	1	-0.5	-0.5	-0.5
	-1	-0.5	-0.5	0.5
	1	-0.5	0.5	0.5
f_{22}	-1	0.5	-0.5	-0.5
	1	0.5	0.5	0.5
	-1	0.5	0.5	0.5
f_{23}	1	-0.5	-0.5	0.5
	-1	-0.5	0.5	-0.5
f_{33}	1	0.5	-0.5	-0.5
	-1	0.5	-0.5	0.5
	1	0.5	0.5	0.5

Table 2: Phantom 2 - Sharp

i	j	I_1	I_2	I_3
1	1	[-0.4,0.4]	[-0.6,0.2]	[-0.8,0.8]
1	2	[-0.4,0.4]	[-0.2,0.6]	[-0.8,0.8]
1	3	[-0.8,0.8]	[-0.4,0.4]	[-0.6,0.2]
2	2	[-0.8,0.8]	[-0.4,0.4]	[-0.2,0.6]
2	3	[-0.6,0.2]	[-0.8,0.8]	[-0.4,0.4]
3	3	[-0.2,0.6]	[-0.8,0.8]	[-0.4,0.4]

8.2.2 Phantom 2: sharp

Phantom 2 is constructed to contain sharp edges, to highlight non-linear strain fields which is not quite compatible with the reconstruction algorithm. As in the smooth case, we define f on the cube $[-1, 1]^3$, but set f_{ij} to be the characteristic function of $I_1 \times I_2 \times I_3$, according to Table 2.

8.3 Reconstruction Procedure

The recovery of *axial* components are relatively straight forward as this is just plane-by-plane Radon inversion. Hence, we apply a ramp-filter (Ram-Lak) to the data and back-project to achieve the diagonal entries for each rotation axis. Since, we can think of back-projection as the dual operator of ray integration, we reuse the ray tracing code to implement back-projection as the transpose of ray integration.

From (36), we see that the simulated data values J^1 that are collected for each plane need to be differentiated in the p -direction, before any back-projection takes place. To implement this, we perform a regularised derivative, which we carry out

in the Fourier domain using a Hamming window regularisation. After performing a one-dimensional Discrete Fourier Transform using the Fast Fourier Transform FFT algorithm, we multiply by $-ikw(n)$, where $w(n)$ is the Hamming window. For a discrete signal of length N , labelled by $n = 0, \dots, N - 1$, the *Hamming window* $w(n)$ is given by

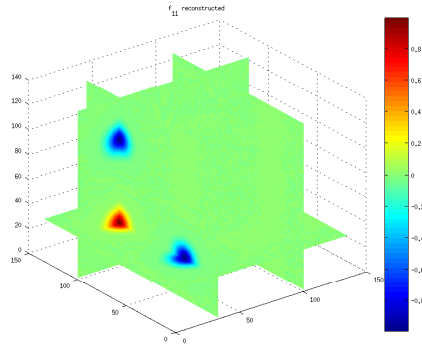
$$w(n) = 0.54 - 0.46 \cos \left(\frac{2\pi n}{N - 1} \right). \quad (59)$$

The result is returned to the spatial domain using the inverse FFT algorithm.

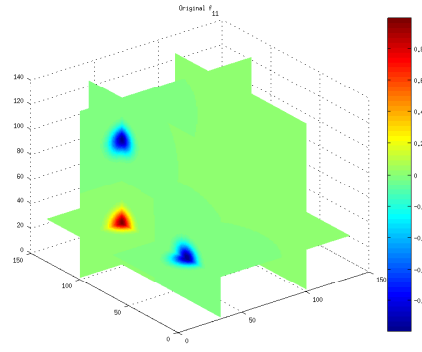
Following the filter we back-project the differentiated plane by plane data onto the voxel grid and the tangential vector field components (i.e. λ) are calculated using a three dimensional FFT algorithm and application of a *ramp-filter* in frequency space. Then equations (41) are used to recover the off-diagonal terms in frequency space. The only exception is the voxel $(y_1, y_2, y_3) = (0, 0, 0)$, where $\hat{f}_{12}, \hat{f}_{13}$ and \hat{f}_{23} are undefined. Here, the value is set using linear interpolation from nearby voxels. To complete our reconstruction, we employ the three dimensional inverse FFT to recover f_{ij} .

8.4 Results and summary

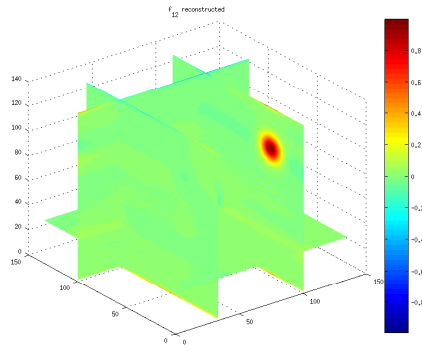
Below we illustrate the results of our implemented reconstructions which clearly show the performance of the algorithm on two different tensor fields. As expected, the smooth (Gaussian) field is reconstructed well. However, when we introduce sharp edges in the components of a field such as a crack, we see that as expected the reconstruction is inaccurate and artefacts are visible. The artefacts increase as more noise is added.



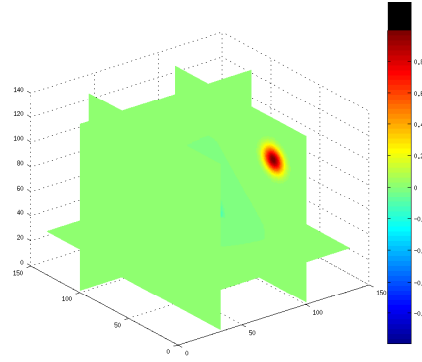
(a) Reconstruction of f_{11}



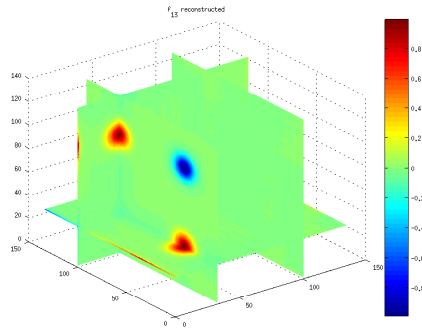
(b) Original f_{11}



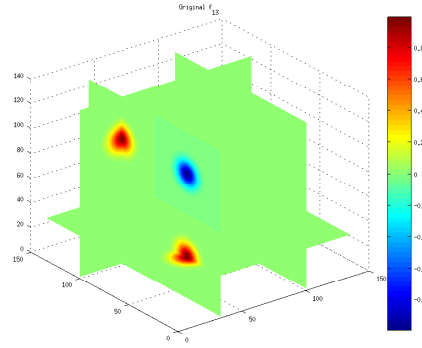
(c) Reconstruction of f_{12}



(d) Original f_{12}

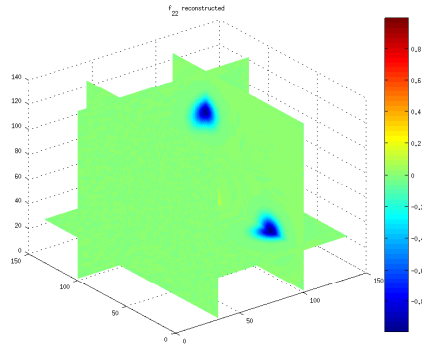


(e) Reconstruction of f_{13}

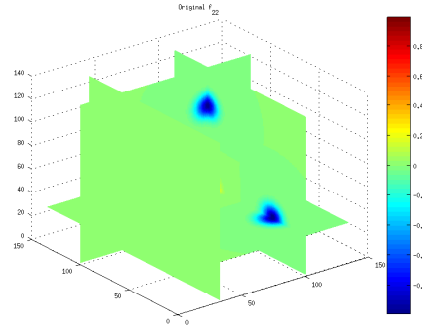


(f) Original f_{13}

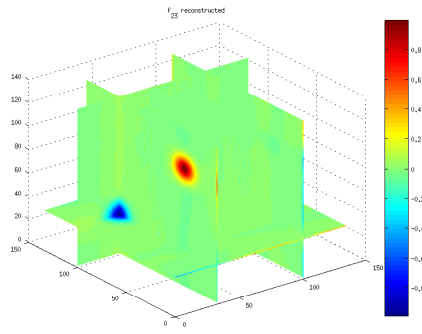
Figure 1: Reconstruction of several gaussian balls f_{11}, f_{12} and f_{13}



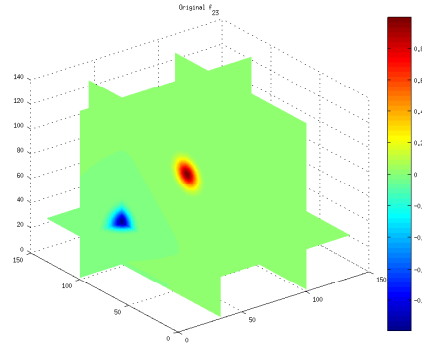
(a) Reconstruction of f_{22}



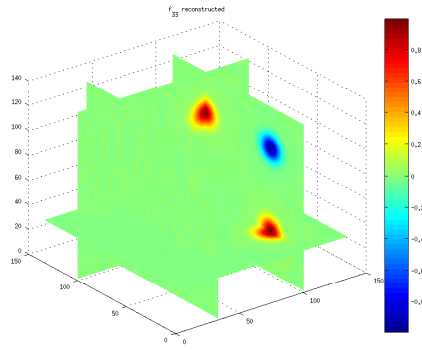
(b) Original f_{22}



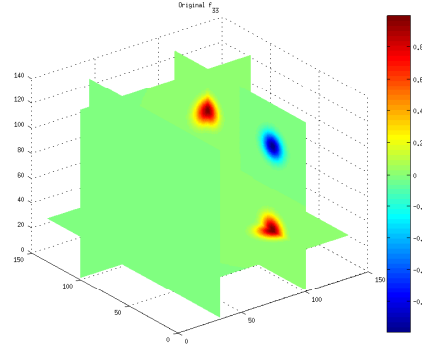
(c) Reconstruction of f_{23}



(d) Original f_{23}

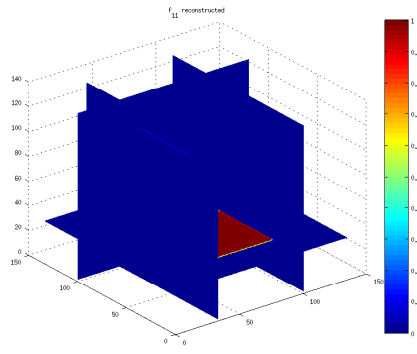


(e) Reconstruction of f_{33}

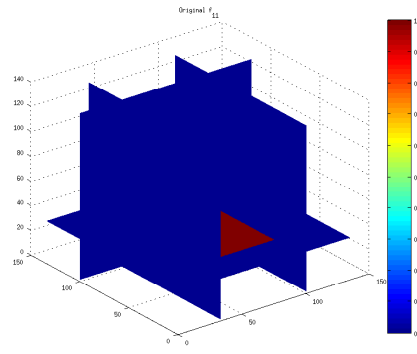


(f) Original f_{33}

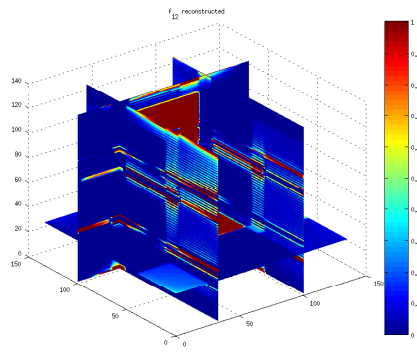
Figure 2: Reconstruction of several gaussian balls for f_{22} , f_{23} and f_{33}



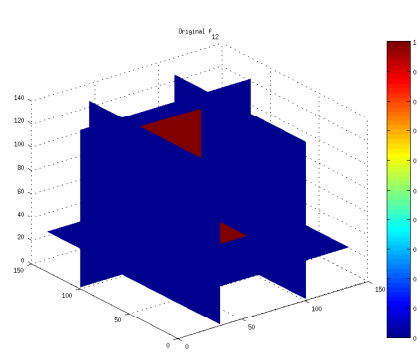
(a) Reconstruction of f_{11}



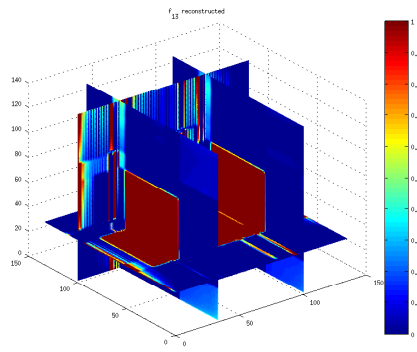
(b) Original f_{11}



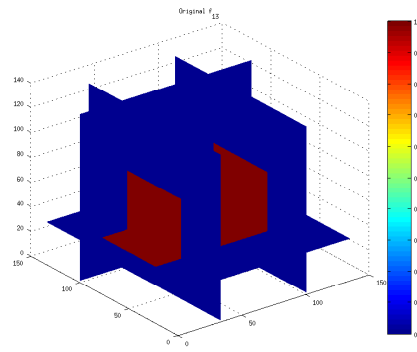
(c) Reconstruction of f_{12}



(d) Original f_{12}

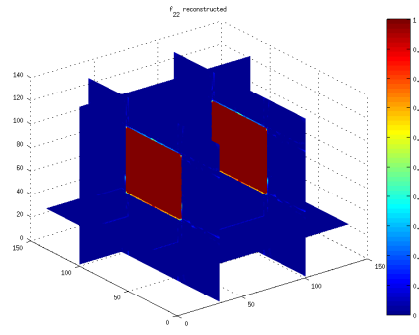


(e) Reconstruction of f_{13}

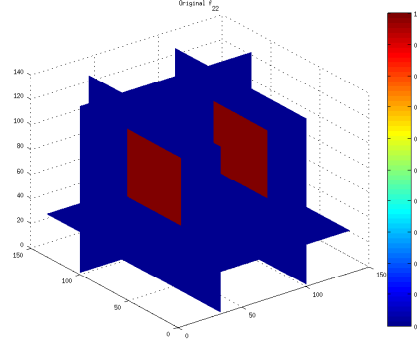


(f) Original f_{13}

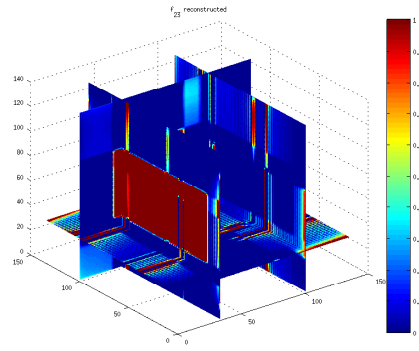
Figure 3: Reconstruction of sharp phantom, f_{11} , f_{12} and f_{13}



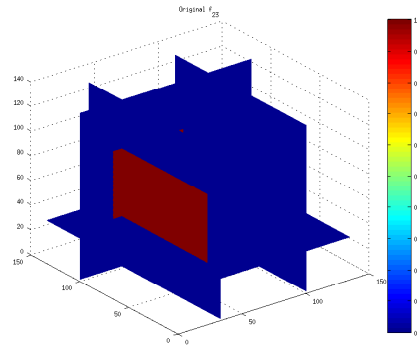
(a) Reconstruction of f_{22}



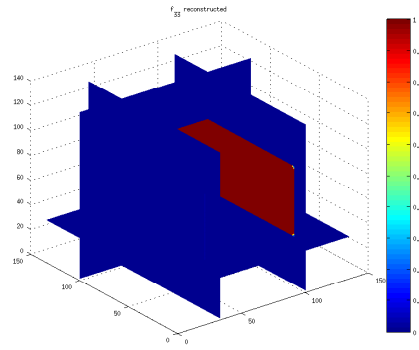
(b) Original f_{22}



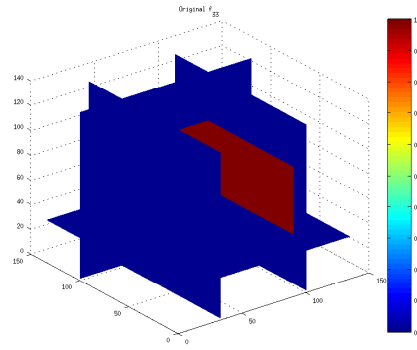
(c) Reconstruction of f_{23}



(d) Original f_{23}



(e) Reconstruction of f_{33}



(f) Original f_{33}

Figure 4: Reconstruction of sharp phantom, f_{22} , f_{23} and f_{33}

9 Conclusions and further work

Overall the procedure we describe would provide an efficient method for x-ray diffraction tomography. It handles smooth tensor fields well but for discontinuous strain fields it would be sensible to try different modified ramp filters or explicit regularization methods such as total variation.

It would be possible in the case of a tensor field that is the result of an infinitesimal strain to use only two axes of rotation, and recover the displacement field directly. However it might be better in practice to use the general procedure and then verify to what extent the compatibility condition holds on the reconstructed tensor.

We have pointed out that as there are two distinct methods of calculating the diagonal components this provides a consistency condition on the data. As the plane-by-plane data is written in terms of scalar, vector and tensor longitudinal ray transforms, and the ranges of these operators can be determined in the plane case as a singular function expansion in a suitable Hilbert space. In fan beam coordinates the singular value decomposition of the ray transform is given by [3]. See also [1] and [2] for a parallel beam formulation.

The Helgason-Ludwig range conditions for the scalar Radon transform in the plane [7, Sec II.4] simply states that the k th moment of the data $\int_{-\infty}^{\infty} s^k Xf(\xi, s\xi^\perp) ds$, when it exists, is a polynomial of degree $\leq k$ in ξ . For the LRT of a rank m tensor the condition is simply degree $\leq k + m$. A deeper connection between these conditions and the singular function expansion is given by [6].

Such consistency conditions, characterizing the range of the forward operator are of great assistance in diagnosing errors and unaccounted for physical effects in experimental data.

Another avenue worth considering on the practical side is to develop a reconstruction algorithm involving general (non-orthonormal) axes. In experiments it is often not feasible to rotate the specimen through 90° and remain in the field of view of the measurement system.

Explicit reconstruction algorithms such as the one we have given are useful practically for data that is complete and uniformly sampled. For partial, sparse or irregularly sampled data representing the forward problem simply as a sparse matrix and solving using iterative algorithms with explicit regularization is generally better, although typically requiring large amounts of memory and parallel processors.

Acknowledgements

Parts of this work were supported by COST Action MP 1207, the Otto Mønstedts Fond, the Royal Society Wolfson Research Merit Award, and EPSRC Grants EP/M022498/1, EP/M010619/1, EP/I01912X/1, P/K00428X/1

References

- [1] E.Y. Derevtsov, A.V. Efimov, A.K. Louis, and T Schuster. Singular value decomposition and its application to numerical inversion for ray transforms in 2D vector tomography. *Journal of Inverse and Ill-posed Problems*, 9:689–715, 2011.
- [2] E.Y. Derevtsov and A.P. Polyakova. Solution of the integral geometry problem for 2-tensor fields by the singular value decomposition method. *Journal of Mathematical Sciences*, 202(1):50–71, 2014.
- [3] S.G. Kazantsev and A.A. Bukhgeim. Singular value decomposition for the 2D fan-beam Radon transform of tensor fields. *Journal of Inverse and Ill-posed Problems*, 12(3):245–278, 2004.
- [4] W.R.B. Lionheart and V.A. Sharafutdinov. Reconstruction algorithm for the linearized polarization tomography problem with incomplete data. In *Imaging microstructures*, volume 494 of *Contemp. Math.*, pages 137–159. Amer. Math. Soc., Providence, RI, 2009.
- [5] W.R.B Lionheart and P.J. Withers. Diffraction tomography of strain. *Inverse Problems*, 31(4):045005, 2015.
- [6] F. Monard. Efficient tensor tomography in fan-beam coordinates. *arXiv:1510.05132v2 [math.AP]*, 2015.
- [7] F. Natterer. *The Mathematics of Computerized Tomography*. Classics in Applied Mathematics. Society for Industrial and Applied Mathematics, 2001.
- [8] V.A. Sharafutdinov. *Integral Geometry of Tensor Fields*. Inverse and ill-posed problems series. VSP, 1994.
- [9] V.A. Sharafutdinov. Slice-by-slice reconstruction algorithm for vector tomography with incomplete data. *Inverse Problems*, 23(6):2603, 2007.
- [10] D. Szotten. *Limited Data Problems in X-ray and Polarized Light Tomography*. PhD thesis, The University of Manchester, Manchester, UK, 1 2011.